Highly accurate measurements of the spontaneous fission half-life of ^{240,242}Pu

P. Salvador-Castiñeira,* T. Bryś, R. Eykens, F.-J. Hambsch,† A. Moens, S. Oberstedt, G. Sibbens, D. Vanleeuw, and M. Vidali
European Commission, Joint Research Centre, Institute for Reference Materials and Measurements (JRC-IRMM), Retieseweg 111, B-2440 Geel, Belgium

C. Pretel
Institute of Energy Technologies, Technical University of Catalonia, Avinguda Diagonal 647, E-08028 Barcelona, Spain
(Received 11 September 2013; published 18 December 2013)

Fast spectrum neutron-induced fission cross-section data for transuranic isotopes are of special demand from the nuclear data community. In particular highly accurate data are needed for the new generation IV nuclear applications. The aim is to obtain precise neutron-induced fission cross sections for ^{240}Pu and ^{242}Pu. To do so, accurate data on spontaneous fission half-lives must be available. Also, minimizing uncertainties in the detector efficiency is a key point. We studied both isotopes by means of a twin Frisch-grid ionization chamber with the goal of improving the present data on the neutron-induced fission cross section. For the two plutonium isotopes the high α-particle decay rates pose a particular problem to experiments due to piling-up events in the counting gas. Argon methane and methane were employed as counting gases, the latter showed considerable improvement in signal generation due to its higher drift velocity. The detection efficiency for both samples was determined, and improved spontaneous fission half-lives were obtained with very low statistical uncertainty (0.13% for ^{240}Pu and 0.04% for ^{242}Pu): for ^{240}Pu, $T_{1/2,SF} = 1.165 \times 10^{11}$ yr (1.1%), and for ^{242}Pu, $T_{1/2,SF} = 6.74 \times 10^{10}$ yr (1.3%). Systematic uncertainties are due to sample mass (0.4% for ^{240}Pu and 0.9% for ^{242}Pu) and efficiency (1%).

DOI: 10.1103/PhysRevC.88.064611 PACS number(s): 25.85.Ca, 28.20.−v, 29.40.Cs

I. INTRODUCTION

In a recent assessment of target accuracies and uncertainties, the Nuclear Energy Agency of the Organisation for Economic Co-operation and Development highlighted the need for improved nuclear data to be used in model calculations for innovative reactor systems (Generation IV) [1]. In this paper the neutron-induced fission cross sections of ^{240,242}Pu were identified as being of highest priority for fast neutron spectrum reactors. Their target uncertainties are very stringent and are requested to be 1–2% for ^{240}Pu and 3–5% for ^{242}Pu from current uncertainties of 6% and 20%, respectively.

In the frame of the Accurate Nuclear Data for Nuclear Energy Sustainability (ANDES) Collaboration, several actinides are under study, among them ^{240,242}Pu. Different experimental methods are being used to determine their neutron-induced fission cross section. For the first time the new digital data acquisition technique was applied for cross-section measurements. Using digital electronics and storing the full waveform opens up new analysis possibilities not available using regular analog electronics.

In the present work we focus on the determination of the fission fragment loss, on the detection efficiency, and on the spontaneous fission half-life, important ingredients in the final neutron-induced fission cross-section determination, which is the subject of a forthcoming paper.

The spontaneous fission half-life is a especially crucial parameter in the final fission cross-section determination. Measurements of this quantity, e.g., for ^{242}Pu, have been performed since the mid-1950s. Many different techniques have been used to determine the spontaneous fission half-lives of both isotopes, and in 2000 Holden and Hoffman [2] made an evaluation of the existing literature for many isotopes and gave recommended values. In the evaluation by Holden and Hoffman, actually all of the papers published before 1967 for ^{240}Pu and a few of the experiments for ^{242}Pu were not used. The reason, definitely for ^{240}Pu, could have been the very high α activity of the sample, causing experimental difficulties in measuring the spontaneous fission half-life. Most of the other results show rather large error bars, again mainly for ^{240}Pu but also some for ^{242}Pu, although the recommended values for both isotopes have uncertainties of about 1% [2]. A new evaluation made by Chechev *et al.* in 2005 [3] and updated in 2009 [4] has come to our knowledge recently, which gave slightly different recommended values and increases the uncertainties on the values to 1.7% for ^{240}Pu and 1.4% for ^{242}Pu. Those values are taken up in Table IV. Details are given in Sec. IV.

II. EXPERIMENTAL SETUP

A twin Frisch-grid ionization chamber (TFGIC) was chosen as the fission fragment (FF) detector. Its characteristics (radiation resistance, solid angle of nearly $2 \times 2\pi$, and good energy resolution) made this type of detector the excellent choice for performing direct kinematics fission experiments. The advantage of using a TFGIC compared to a parallel plate ionization chamber is the fact that by shielding the grid from the anode it is possible to determine the emission angle of the FFs simultaneously with their pulse height (PH). This fact is a key point in the current experiment.

*Also at Institute of Energy Technologies, Technical University of Catalonia, Avinguda Diagonal 647, E-08028 Barcelona, Spain.
†franz-josef.hambsch@ec.europa.eu

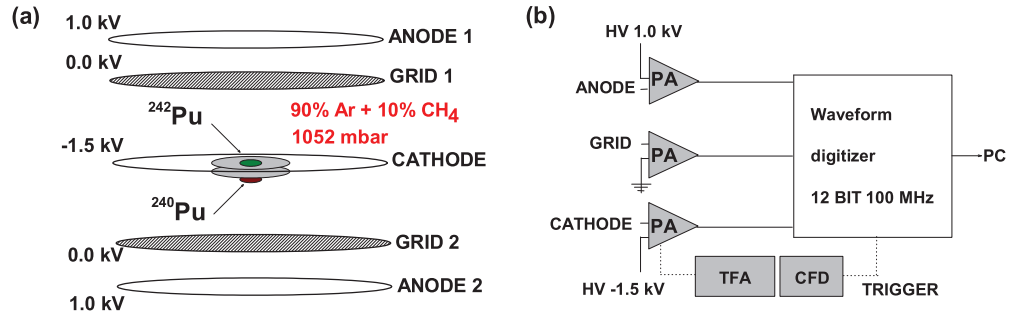

FIG. 1. (Color online) (a) Schematic drawing of a twin Frisch-grid ionization chamber with the two samples inside. (b) Scheme of the electronics for one chamber side.

A schematic representation of the setup is presented in Fig. 1. Because the two samples used in this study have a thick backing, allowing just one FF to be detected, they were placed in back-to-back geometry. The TFGIC was filled with argon methane (P10; 90% Ar + 10% CH_4) as a counting gas at a pressure of 1052 mbar with a constant flow of ∼50 ml/min. The cathode-grid distance was 31 mm and the grid-anode distance was 6 mm, allowing the FFs to be fully stopped within the space between the cathode and the grid. The cathode was common for the two samples and was set at a high voltage (HV) of −1.5 kV, while the two anodes were set at 1 kV. Both grids were grounded. The voltage was chosen to fulfill the condition that the anode-grid electric field strength was three times stronger than the one for the cathode-grid in order to minimize electron losses on the grid. Grids and anodes were connected to charge-sensitive preamplifiers, and the output was fed into a 12-bit 100-MHz waveform digitizer (WFD). The cathode was connected to a current-sensitive preamplifier. The output signal was split: one signal was fed into the WFD and the other was treated with a timing filter amplifier and a constant fraction discriminator resulting in the trigger signal for all the WFDs.

The Pu samples used in this experiment were produced by the so-called *molecular plating* technique in the target preparation laboratory of the JRC-IRMM. The Pu layers have a diameter of 29.95 mm (0.1%) and are deposited on an Al backing with a thickness of 0.25 mm and a diameter of 50 mm. Owing to the short α half-life of the ^{240}Pu, 6561 yr (0.1%), the sample was made to minimize its α activity. Thus, the ^{240}Pu sample has a mass of 92.9 μg (0.4%) and an α activity of 0.8 MBq (0.4%). The ^{242}Pu has an α half-life longer than 1×10^5 yr; for this reason more material could be deposited on top of the disk, with its mass of 671 μg (0.9%) and its α activity of 0.1 MBq (0.3%). Although the accuracy on the determination of the α activity is smaller, the main contribution to the mass uncertainty of ^{242}Pu is due to its α half-life and its uncertainty, 3.75×10^5 yr (0.5%). The activity of both samples was determined by defined solid angle α-particle counting. Their masses were calculated from the activity. The purity of the samples is higher than 99.8% and their atomic abundances were measured by mass spectrometry. To quantify the amount of fission fragments that will be fully stopped in the sample it is important to know the total sample mass. Assuming that the Pu deposits are hydroxides in the form of $Pu(OH)_4$, we calculated the total areal density of the deposit using the measured Pu areal density. This increases the absolute sample thickness by about 28%. The main characteristics of the ^{240,242}Pu samples are summarized in Table I [5].

III. DATA ACQUISITION AND TREATMENT

In the TFGIC, when one of the two isotopes fissions spontaneously, one FF leaves the target and enters into the counting gas. It ionizes the gas particles in its path, generating an electron-ion cloud. The ions travel toward the cathode and the much faster electrons toward the grid. The grid shields (almost perfectly) the anode from the cloud. Once the electrons start to pass the grid, the anode collects the charge. Because of this shielding effect, the anode signal is proportional to the energy that the FF has deposited in the gas, while the grid

TABLE I. Main characteristics of the ^{240,242}Pu samples [5]. All the uncertainties are expanded with a coverage factor $k = 1$. The expanded uncertainty of the sample purity has a coverage factor $k = 2$.

	^{240}Pu	^{242}Pu
Method	Molecular plating	Molecular plating
Chemical composition (assumed)	$Pu(OH)_4$	$Pu(OH)_4$
Total mass (μg) (calculated)	119.22 (0.4%)	859.54 (0.9%)
Total areal density (μg/cm^2) (calculated)	16.9 (0.4%)	122 (0.8%)
Backing	Aluminum	Aluminum
Mass (μg)	92.9 (0.4%)	671 (0.9%)
Areal density (μg/cm^2)	13.19 (0.4%)	95.3 (0.8%)
α-activity (MBq)	0.780 (0.4%)	0.0984 (0.3%)
Purity	99.8915(18)%	99.96518(45)%

signal is proportional to both the energy and the emission angle of the FF.

By using WFDs, the information that is recorded is the raw signal after the preamplifiers. The length of the signal was chosen to be 10 μs, 5 μs before the FF signal and 5 μs after. Within this time frame, and due to the high α activity of our samples, it is likely that more than one α particle will be piled up in the baseline of the preamplifier signal and/or within the FF signal.

The rise time of a typical anode signal is around 0.20 μs when P10 is employed as the counting gas. From the α activity of the samples it is known that the ^{240}Pu emits 0.8 α/μs and the ^{242}Pu, 0.1 α/μs. Considering that the α-particle emission follows a Poisson distribution, we can estimate the amount of α particles that can pile up in the baseline of the signal trace and in the FF slope from the preamplifier. For the ^{240}Pu, we should expect to have in most of the cases between two and five α particles piled up in the baseline before the FF and the same amount in the baseline after the FF event. The case of ^{242}Pu is less severe and we can expect to have zero to two α particles piled up in the baseline before the FF and the same amount after. If now we analyze the actual probability that a FF is detected together with one α particle, we should expect around 14% of these events in the case of ^{240}Pu and just 2% in case of ^{242}Pu. In the case of the grid signal, where its rise time is twice as long as the anode rise time, the probability of having an α particle within the FF signal is 23% for ^{240}Pu and 4% for ^{242}Pu, respectively.

A. α pile-up correction

As explained before, one of the main challenges of this experiment is the high α activity of the samples, particularly that of ^{240}Pu. The use of digital electronics enabled us to optimize the analysis of individual signals and to perform an α pile-up correction.

Figures 2 and 3 present correlated grid and anode signals for the two isotopes. The thick line corresponds to the original signal (the arrows show possible α pile-up signals), while the dash-dotted line is after the α pile-up correction. This shows

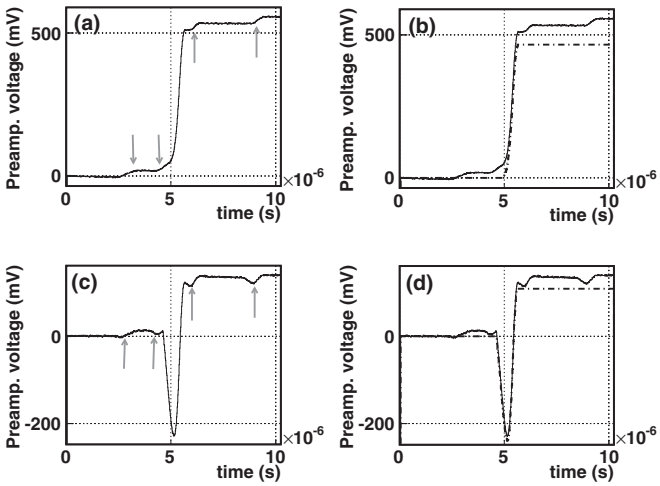

FIG. 2. Typical (a, b) anode and (c, d) grid signals for ^{242}Pu (0.1 MBq): (a, c) raw signals (thick line) with identification of α particles (arrows) and (b, d) signals after α pile-up correction (dash-dotted line).

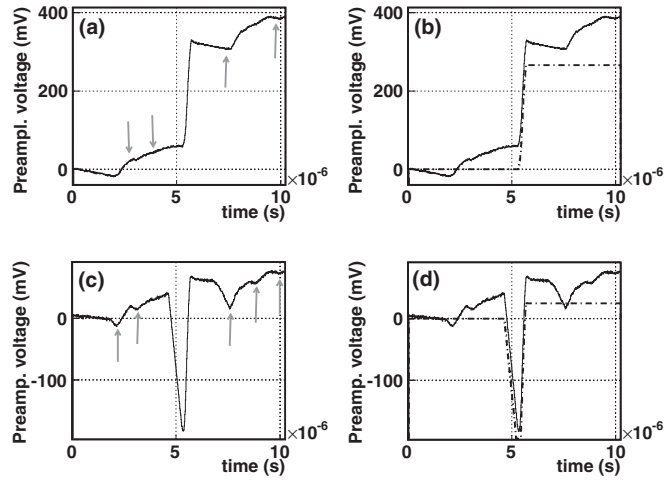

FIG. 3. Typical (a, b) anode and (c, d) grid signals for ^{240}Pu (0.8 MBq): (a, c) raw signals (thick line) with identification of α particles (arrows) and (b, d) signals after α pile-up correction (dash-dotted line).

that most of the α pile-up can be corrected for, leaving a clean signal for further digital processing.

B. Efficiency determination: Fission fragment loss in the sample

Although the TFGIC has a nearly $2 \times 2\pi$ efficiency, our samples are disks with a diameter (30 mm) several orders of magnitude larger than its thickness (0.015 μm for ^{240}Pu and 0.11 μm for ^{242}Pu). Hence, when a FF is emitted close to 90°, it will need to travel a distance up to the diameter of the sample before being emitted into the counting gas. Because the range of a FF inside a transuranic actinide is only a few micrometers, it is unlikely that this FF will enter the counting gas. Therefore, the FF loss inside the sample needs to be quantified as an important correction to the final count rate. In the next section the determination of the fission fragment loss is shown to provide us valuable information on the experimental analysis.

1. Angle determination

One of the properties of spontaneous fission (SF) is that its emission is fully isotropic. By determining the angular distribution of the FF for each sample one should be able to account for the FF loss in the sample comparing the distribution measured with an ideal distribution, as presented in Ref. [6]. The grid signal was used to determine the angular information according to Refs. [7,8]. Figure 4 is a two-dimensional (2D) representation of the grid PH versus the anode PH; the colors indicate a logarithmic scale of the number of detected events. Comparing Figs. 4(a) and 4(b), it is obvious to observe a degradation at low values of the grid PH and at the α region of the ^{240}Pu distribution with respect to the one of ^{242}Pu.

The cosine distribution was determined after correcting the anode and the grid PH for the grid inefficiency. Following the equation

$$\cos\theta = \frac{P_{\mathrm{G}}}{P_{\mathrm{A}}\bar{X}/D}, \tag{1}$$

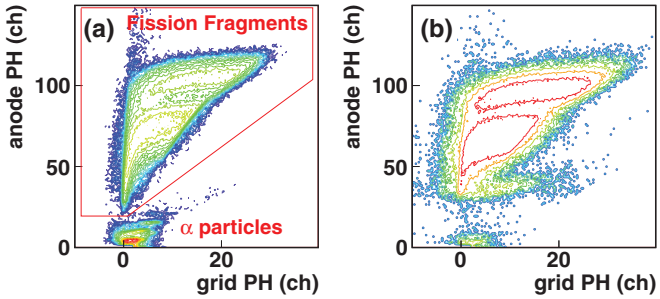

FIG. 4. (Color online) Grid PH versus anode PH for the two isotopes. (a) ^{242}Pu (0.1 MBq); the distinction between α particles and FFs is shown. (b) ^{240}Pu (0.8 MBq)

P_i corresponds to the PH of the anode (A) and the grid (G), $\bar{X}$ is the center of gravity of the electron cloud ionized by the FF, and D is the cathode-grid distance. A 2D distribution (i.e., Fig. 4) of the grid PH versus the anode PH was used to determine the cosine distribution, after excluding the α-particle signals with a region of interest and selecting only the FFs. By selecting regions in the anode PH and projecting them onto the grid PH axis, we can determine the relation between the angle of emission and the grid PH for each anode PH. In this projection, the fragments emitted at 90° will have a grid PH close to zero, while the maximum values for the grid correspond to fragments emitted in the forward direction. The angular distribution obtained is shown in Fig. 5(a). The degradation due to FFs stopped inside the sample and those below the electronic threshold is visible at low cosine values. To determine the total number of emitted FFs ($N_{\cos}$), one would perform

$$N_{\cos} = A + \Delta A, \tag{2}$$

where A is the integral of the cosine distribution and ΔA the missing part related to the thickness of the sample. To extract the sample loss it is necessary to consider the anode PH distribution (N_{PH}) and extrapolate down to zero (ΔN_{PH}) to account for FFs emitted but not detected due to the high electronic threshold requested not to trigger on α events [Fig. 5(b)]. The experimental efficiency due to sample loss

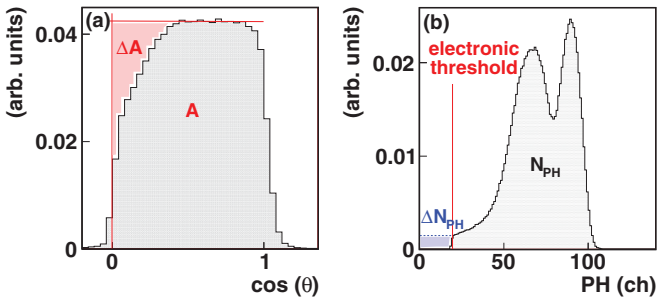

FIG. 5. (Color online) (a) Angular distribution for ^{242}Pu. The FF loss inside the sample is visible at low $\cos\theta$ values. By determining the integral of the distribution and ΔA (the missing part of the distribution) one can obtain the sample loss. (b) PH distribution for ^{242}Pu and determination of the counts under the electronic threshold.

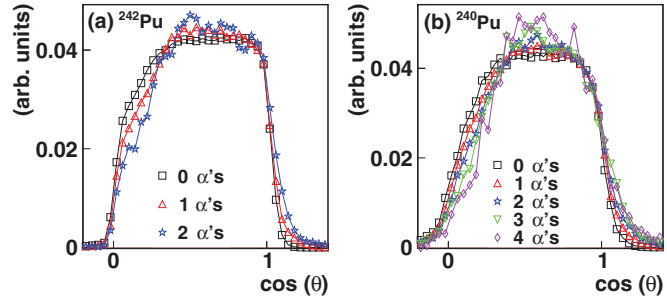

FIG. 6. (Color online) Correlation between α-particle pile-up before the FF event and the degradation of the cosine distribution for (a) ^{242}Pu and (b) ^{240}Pu using P10 as a counting gas. A stronger effect is seen for the more active target (^{240}Pu).

(ϵ_{expt}) is calculated as follows:

$$\epsilon_{\mathrm{expt}} = \frac{N_{\mathrm{PH}} + \Delta N_{\mathrm{PH}}}{N_{\cos}} = \frac{N_{2\pi}}{N_{\cos}}. \tag{3}$$

By performing this analysis for the two isotopes, we obtained an ϵ_{expt} ranging from 94% to 95% with an uncertainty of 1% for the ^{242}Pu and an uncertainty of 94% ± 1% for the ^{240}Pu. However, one would expect that the loss for the thicker sample (^{242}Pu) was more severe than for the thinner one (^{240}Pu). A careful look at the signals of ^{240}Pu presented in Fig. 3 shows that the preamplifiers of the anode and the grid were not completely discharged when the FF event occurred as a consequence of the high α activity. The consequence of this effect is that neither the energy collected nor the angle detected are the correct ones, even though the information that a FF has been detected is correct. This effect is strongly related to the α activity of the sample; the stronger this value, the higher is the effect.

To highlight this, Fig. 6 shows a representation of the cosine distributions of both ^{240,242}Pu as a function of α particles piled up prior to the FF event. Considering that just 10 μs were recorded, it is not possible for us to have a quantitative estimation of the long-term charge that the preamplifiers are receiving due to α particles and that might modify the baseline of the preamplifier output signal. Nevertheless, we see a strong correlation with the amount of α particles piled up in the baseline before the FF event and the degradation of the cosine distribution. This effect has no relevance when the pile-up has occurred after the FF signal.

In addition, we conclude from Fig. 6 that the cosine distribution obtained by choosing the events that had no α pile-up is closer to an ideal distribution. If we instead used this distribution to calculate the sample efficiency the results would be 97% ± 1% for the ^{240}Pu and from 95% to 96% ± 1% for the ^{242}Pu. The results obtained with this distribution are hereafter referred to as the *0-α method*.

2. *Improving the signal rise time: P10 versus CH$_4$*

The rise time of the preamplifiers used in the experiment is faster than 12 ns and, thus, much shorter than the anode signal rise time (0.20 μs); therefore, the only way to verify the behavior explained in the previous section would be to change

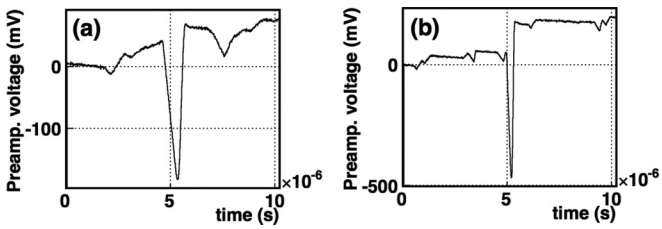

FIG. 7. Grid signals obtained with ^{240}Pu using either (a) P10 or (b) CH_4. A big improvement is seen in the signal taken with CH_4, which can discriminate between nearby α particles.

the counting gas to one with a much higher electron drift velocity. Hence, we chose CH_4 because it has a twofold higher drift velocity than P10 [9]; this gas was already studied as a counting gas in a TFGIC in Ref. [10]. The HV was increased to be in the plateau region on the electron drift velocity and to meet the requirement that the grid-anode field strength is three times the cathode-grid one. For these reasons, 1.5 kV was used for the anodes and −2.5 kV for the cathode. The grids were grounded.

Figure 7 presents a typical grid signal obtained for ^{240}Pu with P10 [Fig. 7(a)] and with CH_4 [Fig. 7(b)]. From the figure it is clearly visible that with pure methane as the counting gas the α-particle signals are well discriminated and the preamplifier is able to discharge almost completely before the next particle enters the counting gas. In addition, the FF signal itself has less probability to suffer from pile-up within the rise time.

The rise time of the anode signals is around 0.077 μs for CH_4 (0.20 μs for P10). As mentioned from the α-particle activity of the samples, the ^{240}Pu emits 0.8 α/μs and the ^{242}Pu 0.1 α/μs. In our trace analysis we are able to correct nearly all the α-particle signals pre- and post-FF. Yet, it is nearly impossible to distinguish and correct for those α-particle signals that are piled up within the FF signal. The probability of an α-particle signal within the frame of the FF in the anode is ∼6% (14%) for ^{240}Pu and ∼0.8% (2%) for ^{242}Pu using CH_4 (P10) as a counting gas. In the case of the grid (where the FF signal is twice as long) the probability is ∼11% (23%) for ^{240}Pu and ∼1.5% (4%) for ^{242}Pu using CH_4 (P10).

Figure 8 depicts the 2D distribution of the grid PH versus

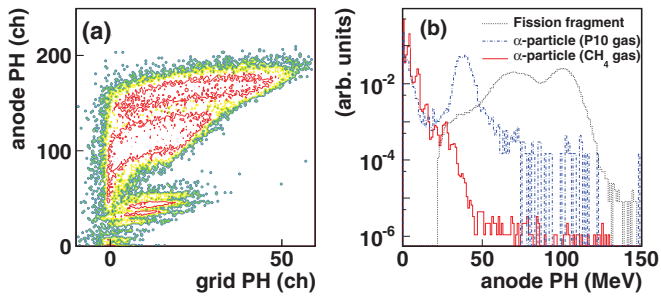

FIG. 8. (Color online) Distributions for ^{240}Pu. (a) 2D grid PH vs anode PH distribution using CH_4 as a counting gas. Three α pile-up lines are visible for anode PH values between channels 20 and 50. (b) Projection of the anode PH when just FFs are selected (dotted line) using either P10 or CH_4, when just α particles are selected and P10 is used as a counting gas (dash-dotted line), and when just α particles are selected and CH_4 is used as a counting gas (solid line).

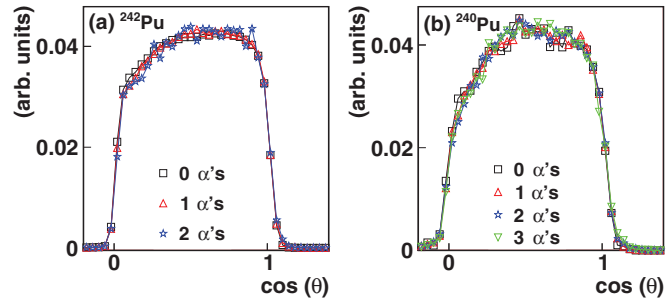

(a)^{242}Pu (0.1 MBq) (b)^{240}Pu (0.8 MBq)

FIG. 9. (Color online) Correlation between α pile-up before the FF event and the degradation of the cosine distribution for (a) ^{242}Pu and (b) ^{240}Pu using CH_4 as a counting gas.

the anode PH obtained with ^{240}Pu using CH_4 as a counting gas. Comparing the present figure with Fig. 4, obtained with P10, it is visible how the degradation on the ^{240}Pu distribution is considerably improved now. By performing the projection onto the anode PH axis, and after normalizing the channels to PH energy, seven distinct α pile-up lines are visible when CH_4 is used as a counting gas (solid line). Those lines correspond to one α particle (∼5 MeV), two α particles (∼10 MeV), etc. In the same plot, we can see the projection of the P10 distribution (dash-dotted line) where just one α pile-up line is visible at around 38 MeV. The dotted line shows the FF PH distribution cleaned of α particles.

By correlating again the amount of α particles before the FF signal and the cosine distribution (Fig. 9), even though the statistics at higher α pile-up for ^{240}Pu are low, we observe an improvement with respect to Fig. 6. The analysis gives an ϵ_{expt} ranging from 98% to 100% with an uncertainty of 1% for both samples. The accuracy that this method can provide is not better than 1% in any case. This is based on the fact that analyzing different runs for both gas mixtures and samples gives slightly different cosine distributions. This is exemplified in Fig. 10.

A different experimental method (*ideal*) can be applied for determining the sample efficiency by means of the cosine distribution. The method consists of considering an ideal continuous uniform cosine distribution in the range $\cos\theta =$

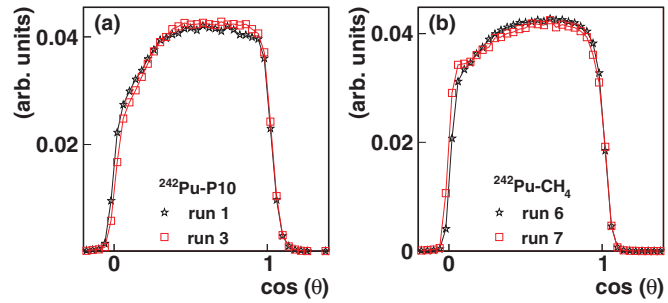

FIG. 10. (Color online) Comparison of the cosine distributions for different runs for ^{242}Pu using (a) P10 and (b) CH_4. We observed that for two different runs with the same isotope and counting gas slightly different cosine distributions are obtained; therefore, with these methods it is not possible to achieve an accuracy better than 1%.

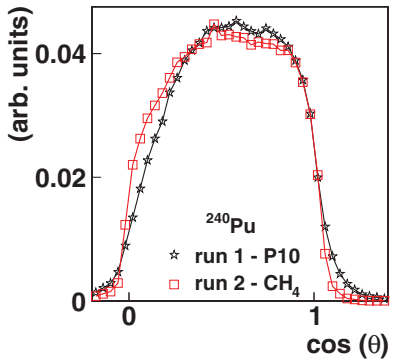

FIG. 11. (Color online) Comparison of the cosine distributions of ^{240}Pu obtained using P10 and CH_4 (see text for further explanation).

TABLE II. Summary on the efficiency (ϵ) results by using different methods, counting gas, and cosine distributions.

Description				
Cosine distribution	Method	Counting gas	^{240}Pu	^{242}Pu
All events	Ref. [6]	P10	94% ± 1%	94–95% ± 1%
All events	Ideal	P10	99.6% ± 1%	98–99% ± 1%
0-α	Ref. [6]	P10	97% ± 1%	95–96% ± 1%
0-α	Ideal	P10	100% ± 1%	99% ± 1%
All events	Ref. [6]	CH_4	98–100% ± 1%	98–100% ± 1%
All events	Ideal	CH_4	∼100% ± 1%	∼100% ± 1%
	Theory		99.7%	98.1%
	GEANT4		99.2%	97.4%

[0, 1], where the normalized counts in each bin should be equally distributed along the range. We take as an example Fig. 11, where two distributions of ^{240}Pu are shown, the first one obtained with P10 and the second one with CH_4. In our ideal case the maximum value of the distribution corresponds to the normalized total amount of counts divided by the number of bins in the range, in that case 0.04. One can easily notice that the maximum value of the distribution taken using P10 as a counting gas is well above 0.04. By using CH_4 as a counting gas, the maximum value of the distribution is slightly lower than for P10 but still higher than the ideal 0.04; as a consequence one could assume that this difference of counts is equivalent to the lack of counts in the low-cosine-value part (between $\cos\theta = 0$ and $\cos\theta = 0.4$). Taking into account these observations, it is possible to determine the sample efficiency considering that the maximum normalized amount of counts in each bin of the distribution would be the number of bins multiplied by their width. This is in the present case 0.04. In the bins that exceed this value, we would take the difference between the value and the maximum considered value and add these extra counts to the bins with low cosine values. Thus, if we perform once more the recalculation of the $N_{\cos}$ assuming that the level of the distribution is 0.04, the sample efficiency that we would obtain is from 98% to 99% (1%) for the ^{242}Pu and 99.6% (1.0%) for the ^{240}Pu with P10 and around 100% ± 1% for both samples using CH_4.

The 0-α method can be applied together with the ideal method obtaining as a result for the sample efficiency 99% ± 1% for the ^{242}Pu and 100% ± 1% for the ^{240}Pu (using the P10 data). The 0-α method does not improve the result on the CH_4 cosine distributions because in these distributions there is no degradation due to α pile-up.

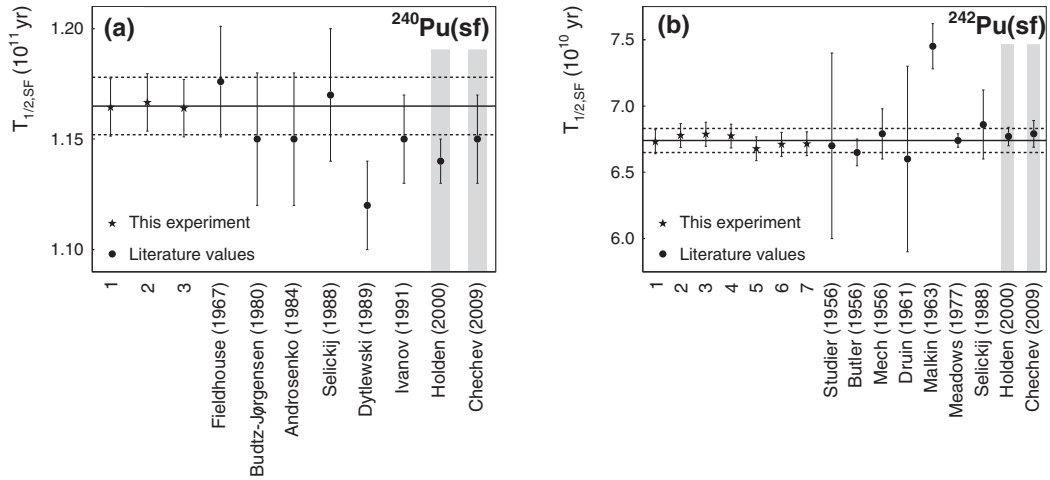

FIG. 12. SF half-life results for (a) ^{240}Pu and (b) ^{242}Pu (stars) compared with some literature values (bullets), their weighted average calculated by Ref. [2] (Holden 2000), and the weighted average calculated by Refs. [3] and [4]. The thick line is the weighted average of all the experimental runs and the dotted lines are the total uncertainty on the weighted average. The mean was weighted by using the statistical uncertainty and then adding the systematic component (1.1% for ^{240}Pu and 1.3% for ^{242}Pu). The literature values shown are the ones used in Refs. [2] and [3] to calculate the weighted average. In the ^{240}Pu case the literature values correspond to studies by Fieldhouse (1967) [14], Budtz-Jørgensen (1980) [15], Androsenko (1984) [16], Selickij (1988) [17], Dytlewski (1989) [18], Ivanov (1991) [19], Holden (2000) [2], and Chechev (2009) [3]. The literature values for the ^{242}Pu are from studies by Studier (1956) (cited by Ref. [20]), Butler (1956) [21], Mech (1956) [20], Druin (1961) [22], Malkin (1963) [23], Meadows (1977) [24], Selickij (1988) [17], Holden (2000) [2], and Chechev (2009) [3].

3. *Results on the sample efficiency*

To verify the efficiency results obtained with the different analysis methods, theoretical calculations using SRIM [11] stopping power ranges and GEANT4 simulations [12] were done. A brief explanation of the two methods is given.

Theoretical calculation. The calculation was done as presented in Ref. [6]. Properties for two typical FFs were used. The loss inside the sample can be calculated as

$$\Delta_{\text{sample}} = \frac{t}{2R_{\text{sample}}} = \frac{t}{2}\sum_i \frac{W_i}{R_i} \tag{4}$$

with t as the thickness of the sample, R_i the range of isotope i, and W_i the weight fraction of isotope i in the sample.

GEANT4 simulations. Simulations with GEANT4 were performed with a FF kinetic energy distribution obtained with the GEF code [13]. From the simulations the transmitted FFs from the sample to the counting gas were obtained.

Table II summarizes the results obtained using different methods and cosine distributions. By changing the counting gas inside the TFGIC, it was possible to overcome almost completely the effect of the loss of information due to an incomplete discharge of the preamplifiers caused by α-particle pile-up. In addition, it is possible to improve the initial results by being able to tag the α particles piled up and use a cosine distribution of the events that had no coincidence with α particles. This is possible just by using digital electronics. If we extrapolate this result, assuming the use of an even faster gas (in terms of drift velocity of the electrons) and preamplifiers with rise time faster than the signal rise time, we could experimentally verify the theoretical value in terms of value and accuracy. In consequence, the theoretical value is the one used for the SF half-life calculation, considering the experimental uncertainty described above (1% for the FF loss for the two samples considered).

IV. SPONTANEOUS FISSION HALF-LIFE

The SF half-life was calculated using the following:

$$T_{1/2,\text{SF}} = \frac{\%^j\text{Pu}}{\text{A}_j}\frac{1}{\left(\frac{C_{\text{SF}}}{t\epsilon_j(\ln 2)m_{\text{Pu}}N_{\text{A}}} - \sum_i^n \frac{\%^i\text{Pu}}{\text{A}_i T_{1/2,\text{SF}}(i)}\right)}, \tag{5}$$

where $\%^j$Pu is the purity of the sample, A_j its atomic mass, C_{SF} are the counts detected, t is the effective measuring time, ϵ_j is the detection efficiency, m_{Pu} is the sample mass, N_A Avogadro's number, and $\sum_i^n \frac{\%^i\text{Pu}}{\text{A}_i T_{1/2,\text{SF}}(i)}$ the contribution from the other isotopes contained in the sample.

TABLE III. Summary of the uncertainties corresponding to the SF half-life ($T_{1/2,\text{SF}}$) for ^{240,242}Pu.

Uncertainty source	^{240}Pu	^{242}Pu
Statistical	0.13%	<0.1%
Mass	0.4%	0.9%
Sample efficiency	1%	1%
Sample purity	<0.001%	<0.001%
Dead time acquisition program	<0.07%	<0.12%
Total (systematic and statistical)	1.1%	1.3%

TABLE IV. Summary of the SF half-life ($T_{1/2,\text{SF}}$) for ^{240,242}Pu. The experimental uncertainties presented are both the statistical and systematic uncertainties. The weighted average of literature values presented by Ref. [2] and by Ref. [3].

$T_{1/2,\text{SF}}$ (yr)	^{240}Pu	^{242}Pu
Holden (2000) [2]	1.14×10^{11} (0.9%)	6.77×10^{10} (1.0%)
Chechev (2009) [3,4]	1.15×10^{11} (1.7%)	6.79×10^{10} (1.4%)
This experiment	1.165×10^{11} (1.1%)	6.74×10^{10} (1.3%)

Several measurements were performed with each sample. Figure 12 summarizes in a graph the resulting $T_{1/2,\text{SF}}$ values. Run 1 for ^{240}Pu and runs 1–5 for ^{242}Pu were performed with P10 as a counting gas, while runs 2 and 3 for ^{240}Pu and runs 6 and 7 for ^{242}Pu were performed with CH_4. Each run contains several individual data sets obtained under the same experimental conditions. The data sets contain between 10 000 and 250 000 fission events using P10 and between 50 000 and 1 500 000 events using CH_4. All labeled runs are performed using a different electronic threshold. The error bars in the plot describe the statistical and the systematic uncertainties, the thick horizontal line is a visual guide for the weighted average of our data, and the dotted lines are the final uncertainties (systematic and statistical) expressed with 1σ. It is worth mentioning that the weighted average was calculated using just the statistical uncertainties and, once the value was obtained, the systematic uncertainties were included in the final value. The bullet symbols represent previous experimental results, and the two highlighted literature values are the weighted average of the subset of literature data presented given by Refs. [2] and [3]. In Table III the present uncertainty budget is listed and Table IV lists the weighted average of our experimental data together with the weighted average of the literature values by Ref. [2] and by Ref. [3].

To clarify the uncertainty budget of previous literature data we have listed it in two tables. Table V describes the data from ^{240}Pu and Table VI data corresponds to ^{242}Pu. It is clear that the present experiment was performed with unprecedented statistics. In addition, we could reach lower systematic uncertainties

TABLE V. Summary of the uncertainties corresponding to the SF half-life ($T_{1/2,\text{SF}}$) of the literature values presented in Fig. 12 for ^{240}Pu. The statistical and systematic uncertainties are given where known together with the total uncertainty. (The hyphen indicates a situation where the uncertainty budget of the experiment is not well described; thus, the total uncertainty is taken.)

Experiment	σ_{STAT}	σ_{SYST}	σ_{TOTAL}
Fieldhouse (1967) [14]	–	2%	2%
Budtz-Jørgensen (1980) [15]	1.5%	2.1%	2.6%
Androsenko (1984) [16]	–	–	2.6%
Selickij (1988) [17]	–	2.5%–3.3%	2.6%
Dytlewski (1989) [18]	0.8%	∼1.4%	1.6%
Ivanov (1991) [19]	–	–	1.7%
This experiment	0.13%	1.1%	1.1%

TABLE VI. Summary of the uncertainties corresponding to the SF half-life ($T_{1/2,SF}$) of the literature values presented in Fig. 12 for ^{242}Pu. The statistical and systematic uncertainties are given where known together with the total uncertainty. (The hyphen indicates a situation where the uncertainty budget of the experiment is not well described; thus, the total uncertainty is taken.)

Experiment	σ_{STAT}	σ_{SYST}	σ_{TOTAL}
Studier (1956) (cited by Ref. [20])	–	–	10%
Butler (1956) [21]	0.8%	1.3%	2.6%
Mech (1956) [20]	∼0.6%	2.6%	2.7%
Druin (1961) [22]	5%	∼8.7%	10%
Malkin (1963) [23]	–	–	2.3%
Meadows (1977) [24]	0.4%–0.5%	∼0.5%	0.7%
Selickij (1988) [17]	∼2.7%	2.7%	3.8%
This experiment	<0.1%	1.3%	1.3%

than most of the previous experiments. In the case of ^{242}Pu, there was one experiment with lower systematic uncertainties (Ref. [24]). In that experiment, the sample preparation as well as the FF detector were similar to the present work. Nevertheless, the considered uncertainty on the fission fragment loss inside the sample is only 0.1%. Hence, their total uncertainty is only 0.7%. Despite of that, our value is the same as the value of Ref. [24] recalculated by Ref. [2], taking into account the new value of the half-life of ^{239}Pu.

Our results are in agreement with the literature values for ^{242}Pu. Nevertheless, and using exactly the same method, the ^{240}Pu SF half-life is slightly higher than some of the literature values. This could be explained by the high α-particle activity of the sample. By having a more precise discrimination of α-particle signals our count rate might have been lower than in previous experiments done with analog electronics, thus obtaining a higher SF half-life value.

V. RESULTS AND CONCLUSIONS

The need for improved neutron-induced fission cross sections of ^{240,242}Pu in the fast neutron spectrum range required a complete study of the behavior of the TFGIC with samples of high α-particle activity by using digital electronics. For the first time, we were able to correlate a degradation of the cosine distribution with the number of α particles piled up in the time frame where the signal was recorded. By changing the counting gas from P10 to CH_4 we were able to considerably improve signal treatment in the event of (multiple) α-particle pile-up and cross-check the efficiency that one can obtain using theoretical calculations and Monte Carlo codes with experimental values. Finally, the spontaneous fission half-lives of ^{240,242}Pu were remeasured with an unprecedented statistical uncertainty smaller than 0.15% and lower systematic uncertainties than previous experiments (see Table IV).

ACKNOWLEDGMENT

One of the authors (P.S.-C.) acknowledges financial support from the ANDES Collaboration (Contract No. FP7-249671).

[1] M. Salvatores, NEA Report No. NEA/WPEC-26, 2008 (unpublished) .
[2] N. Holden and D. Hoffman, Pure Appl. Chem. **72**, 1525 (2000).
[3] V. P. Chechev, in *Proc. Intern. Conf. Nuclear Data for Science and Technology*, edited by R. C. Haight, M. B. Chadwick, T. Kawano, and P. Talou, Vol. 1 (Santa Fé, New Mexico, 2005), p. 91; AIP Conf. Proc. 769 (2005).
[4] http://www.nucleide.org/DDEP_WG/DDEPdata_by_Z.htm.
[5] G. Sibbens, A. Moens, R. Eykens, D. Vanleeuw, F. Kehoe, H. Kühn, R. Wynants, J. Heyse, A. Plompen, R. Jakopiĉ, S. Richter, and Y. Aregbe, J. Radiol. Nucl. Chem. **297** (2013).
[6] C. Budtz-Jørgensen and H.-H. Knitter, Nucl. Sci. Eng. **86**, 10 (1984).
[7] A. Al-Adili, F.-J. Hambsch, R. Bencardino, S. Pomp, S. Oberstedt, and S. Zeynalov, Nucl. Instrum. Methods A **671**, 103 (2012).
[8] O. Zeynalova, S. S. Zeynalov, F.-J. Hambsch, and S. Oberstedt, Bull. Russ. Acad. Sci.: Phys. **73**, 506 (2009).
[9] G. Knoll, in *Radiation Detection and Measurement*, 3rd ed. (New York, Wiley, 2000), p. 133.
[10] F. Tovesson, F.-J. Hambsch, S. Oberstedt, and H. Bax, J. Nucl. Sci. Technol. **2**, 673 (2002).
[11] J. Ziegler, http://www.srim.org/
[12] http://geant4.web.cern.ch/geant4/
[13] K.-H. Schmidt and B. Jurado, GEF code version 2012/2.7, http://www.cenbg.in2p3.fr/-GEF-/
[14] P. Fieldhouse, D. Mather, and E. Culliford, J. Nucl. Energy **21**, 749 (1967).
[15] C.Budtz-Jørgensen and H.-H. Knitter, Euratom Prog. Report No. NEANDC(E)-212-3,5, 1980 (unpublished).
[16] A. Androsenko, P. Androsenko, Y. Ivanov, A. Konyaev, V. Kositsyn, and V. Shchebolev, Sov. J. At. Energy **57**, 788 (1984).
[17] J. Selickij, V. Funstein, and V. Jakovlev, *Proceedings of the 38th Annual Conference on Nuclear Spectroscopy and Structure in Atomic Nuclei, Baku, 1988* (Acad. Sci. USSR, 1988), Vol. 131.
[18] N. Dytlewski, M. G. Hines, and J. W. Boldeman, Nucl. Sci. Eng. **102**, 423 (1989).
[19] Y. Ivanov, A. Konyaev, V. Kositsyn, E. Kholnova, V. Shchebolev, and M. Yudin, Sov. J. At. Energy **70**, 491 (1991).
[20] J. Mech, H. Diamond, M. Studier, P. Fields, A. Hirsch, C. Stevens, R. Barnes, D. Henderson, and J. R. Huizenga, Phys. Rev. **103**, 340 (1956).
[21] J. Butler, M. Lounsbury, and J. Merritt, Can. J. Chem. **34**, 253 (1956).
[22] V. A. Druin, V. P. Perelygin, and G. I. Khlebnikov, Sov. Phys. JETP **13**, 913 (1961).
[23] L. Z. Malkin, I. D. Alkhazov, A. S. Krivokhatskii, and K. A. Petrzhak, At. Energ. USSR **15**, 158 (1963).
[24] J. W. Meadows, BNL-NCS-24273(1978) 10 (A830926).